

Loading rate effect on notched flexural HSC beams

A.L. Rosa

Universidad de Castilla-La Mancha, Ciudad Real, CLM, Spain,

Universidade Estadual de Campinas, Campinas, SP, Brazil

R.C. Yu & G. Ruiz

Universidad de Castilla-La Mancha, Ciudad Real, CLM, Spain

J.L.A.O. Sousa

Universidade Estadual de Campinas, Campinas, SP, Brazil

T.N. Bittencourt

Universidade de São Paulo, São Paulo, SP, Brazil

ABSTRACT: It has been observed in experiments that crack propagation in concrete is influenced by time-dependent mechanisms, not only for dynamic cases but also in quasi-static load regime, where inertia and wave effects are negligible. Those mechanisms introduce a time scale, due to the rate of loading and/or load duration (sustained load). The specific fracture energy and the peak load were observed to undergo increases as the loading rate increases. Accordingly, to study this rate effect, we develop a viscous-cohesive law endorsed with a viscous term dependent on the crack opening rate in a finite element smeared-crack-tip framework. The model is then adopted to simulate experimental results of prismatic HSC notched beams, tested in three-point bend (TPB) configuration, where five loading rates (ranging from 10^{-5} mm/s to 10^1 mm/s) were employed for each set of specimens. Experimental observations are discussed and compared with numerical results obtained by the developed viscous-cohesive model. It seems that numerical simulations shows good resemblance with experiments, particularly for peak load. The model has been used also to perform a parametric study, pointing model trends on peak load and fracture energy.

1 INTRODUCTION

Similar to the viscoelastic behavior of the bulk material, crack propagation in quasibrittle materials like concrete is influenced by time-dependent mechanisms, apart from temperature and moisture content, not only for dynamic cases but also in quasi-static load regime (Gettu & Bažant 1990, Reinhardt & Weerheijm 1991, Bažant & Gettu 1992, Rossi et al. 1992,1994, Bažant & Jirásek 1993, Bažant & Li 1993, Bažant et al. 2000, Brara & Klepaczko 2007, Ruiz et al. 2008, Zhang et al. 2009), where wave and inertial effects are negligible (e.g., the case of cracking in massive concrete structures like dams).

Time-dependent mechanisms introduce an additive time scale, due to the rate of loading and/or load duration (sustained load), such as the specific fracture energy G_F experiments an increase with the increase of the rate of loading. In this context, the material response undergoes a strengthening and the time-independent crack criterion, such as the Fictitious Crack Model (FCM) and the increase of the energy release rate with the structural size increase,

which induces a size effect, describes the fracture behavior just on its simplest manifestation.

In order to simulate this loading-rate influence (rate effect) observed in the experiments performed at those relatively low loading rates (no inertial and waves influence), we propose a rate dependent cohesive model (a viscous cohesive relation) implemented in a finite element smeared crack tip framework (Planas 1986, Planas & Elices 1991, 1992, 1993, Bažant 1990, Bažant & Beissel 1994, Ruiz 2001, Bažant & Zi 2003), so that the nonlinear solution is sought from a triangular system of equations obtained by superposing linear elastic fracture mechanics (LEFM) cases. The proposed viscous cohesive relation couples a viscous parameter, as a function of crack opening rate (\dot{w}), to Hillerborg's fictitious crack propagation to represent a viscous-cohesive fracture process zone (FPZ) in an elastic bulk material.

The paper is organized as follows. In Section 2, we present the proposed viscous-cohesive law with an explanation of the established hypothesis and the calculation procedure. The essential of the experi-

mental program is depicted in Section 3. Calculations are presented in Section 4 and validated against experimental results of prismatic HSC notched beams, tested in three-point bend (TPB) configuration according Ruiz et al. (2008), in which five loading rates, ranging from 10^{-5} mm/s to 10^1 mm/s, were employed for each set of specimens. Conclusions are drawn in Section 5.

2 THE RATE DEPENDENT COHESIVE MODEL

2.1 The viscous cohesive relation

To take into account the rate effect on quasibrittle fracture, we propose a viscous cohesive-law ($\sigma(w, \dot{w})$) dependent on crack opening (w) and crack opening rate (\dot{w}), as follows

$$\sigma(w, \dot{w}) = \left[1 + \left(\frac{\dot{w}}{\dot{w}_o} \right)^n \right] f(w) \quad (1)$$

where w_o is a normalization parameter, n , named index of rate dependence, is a nondimensional constant that describes the degree of viscosity of the material. The function $f(w)$ defines a general static cohesive law. The case of $f(w)$ being bilinear is represented by the dashed line in Figure 1. In Figure 1 the bilinear continuous lines represent possible viscous-cohesive paths as a projection at the nondimensional σ/f_t^s vs. w/w_{ch} plane defined by the viscous cohesive function $\sigma(w, \dot{w})$. As shown in Figure 1, a viscous-cohesive crack initiates when the stress at crack tip reaches the material tensile strength, f_t^s , considered as static, evolving to a critical crack opening value ($w_c = 22.9 \times w_{ch}$ in our simulations) in such a way that crack faces are not able to undergo stresses, i.e., no stress transfer across the crack occurs for $w \geq w_c$. Note that $w_{ch} = G_F^s / f_t^s$ is the characteristic crack opening and G_F^s is the fracture energy, considered as static. The area for $\dot{w} \rightarrow 0$ (shaded area above the dashed line in Fig. 1) represents G_F^s . The areas above the continuous lines represent the apparent fracture energy G_F measured as a function of loading rate.

2.2 Calculation procedure: the smeared crack tip framework

The rate-dependent cohesive law in Equation (1) is implemented in the framework of the finite element smeared crack-tip method (Planas & Elices 1991), which simulates a path defined Mode I cohesive fracture as a superposition of a series of stress-free crack in a linear-elastic body (Fig. 2). In this way the nonlinear fracture response of HSC specimens is written as the sum of N elastic cases corresponding

to N different crack lengths, each one with a stress-free crack with its tip at node j ($j = 1, 2, \dots, N$) and an external incremental load (ΔP_j) (Fig. 2).

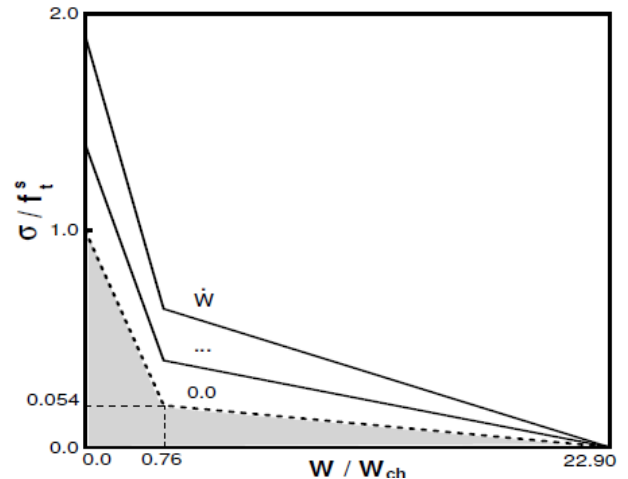


Figure 1. A bilinear rate-dependent cohesive law.

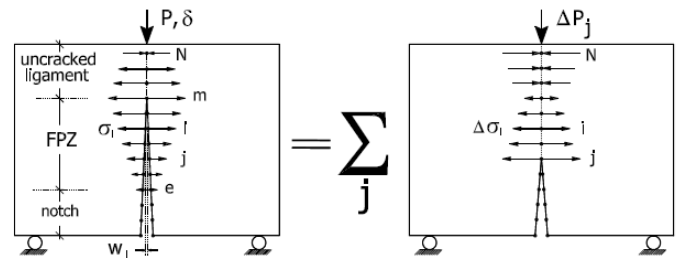


Figure 2. Illustration of the calculation procedure.

The distributions of nodal stresses (σ_i), nodal crack openings (w_i), the total external load (P) and the total displacement (δ) under the load-point can be evaluated by the following equations:

$$\sigma_i = \sum_{j=1}^N R_{ij} \Delta P_j \quad (2)$$

$$w_i = \sum_{j=1}^N D_{ij} \Delta P_j \quad (3)$$

$$P = \sum_{j=1}^N \Delta P_j \quad (4)$$

$$\delta = \sum_{j=1}^N C_j \Delta P_j \quad (5)$$

where: C_j , R_{ij} and D_{ij} are coefficients denoting, respectively, the displacement of the load point, the nodal stress and the crack opening at a node i when a external unit force is applied with a crack reaching node j (see, Fig. 2). Those coefficients can be obtained through a coefficient matrix M , known a priori through any commercial finite element code.

By imposing the boundary conditions and considering the viscous-cohesive law in Equation 1, the nodal stresses (σ_i), the nodal crack openings (w_i), the total external load (P) and the total displacement (δ) of the load-point (Equations (2) - (5)) can be addressed by solving iteratively the nonlinear system of $m - e + 1$ equations given by Equation (6) as follows: starting from an estimate, at an iterative step α of the incremental load $\Delta P_j = \Delta P_j^\alpha$ in the right-hand side and solving for a better estimate $\Delta P_j^{\alpha+1}$ from the left-hand side.

$$\sum_{j=e}^i R_{ij} \Delta P_j^{\alpha+1} = \sigma \left(\dot{w}_i, \sum_{j=i+1}^m D_{ij} \Delta P_j^\alpha \right); i = e, \dots, m \quad (6)$$

In the above equation the nodal crack opening velocity (\dot{w}_i) is obtained through the rate relation:

$$\dot{w}_i^{(j)} = \frac{w_i^{(j)} - w_i^{(j-1)}}{\delta^{(j)} - \delta^{(j-1)}} \dot{\delta} \quad (7)$$

where a dot superscript denote a time derivative; index j corresponds to variables at loading step j and $\dot{\delta}$ is the loading applied rate.

3 EXPERIMENTAL PROGRAM

3.1 TPB tests and material characterization

As aforementioned, we validate the current model against the experimental results performed on notched HSC concrete beams in TPB configuration, according to Ruiz et al. (2008). All of the calculations have been performed using the geometry dimensions shown in Figure 3. The HSC notched beams were tested following, essentially, the RILEM (1985) recommendations and improvements devised by Guinea et al. (1992), Planas et al. (1992), Elices et al. (1992, 1997).

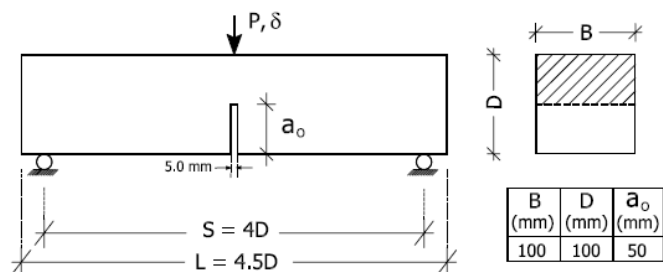


Figure 3. TPB configuration and geometric dimensions.

Independent tests were performed to characterize the high strength concrete (HSC) used in the experiments. The main properties and fracture parameters of the hardened HSC are summarized in Table 1. Measured mean values and standard deviation are

also shown. Note that the static value of the apparent fracture energy, $G_F = G_F^S$, considered as a true material property, was obtained by curve fitting of experimental data from the mean values of the specific fracture energy calculated for each set of specimens subject to the same applied loading rate. Five different loading rates were applied from a quasi-static level (1.74×10^{-5} mm/s and 5.50×10^{-4} mm/s) to a highest level (1.74×10^{-2} mm/s, 5.50×10^{-1} mm/s and $1.74 \times 10^{+1}$ mm/s). In addition, four specimens for each loading rate were employed during the tests.

Table 1. Hardened HSC mechanical properties.

	E_c^*	f_t^{S**}	G_F^{S***}	ℓ_{ch}^{****}	β_H^{*****}
	GPa	MPa	N/m	mm	-
Mean	33.9	5.2	128	160.5	0.62
Std	1.2	0.5	-	-	-

*Cylinder axial compression tests.

**Splitting cylinder (Brazilian) tests.

***Obtained by curve fit of experimental data.

$$**** \ell_{ch} = E_c G_F^S / (f_t^S)^2.$$

$$***** \beta_H = D / \ell_{ch}.$$

4 NUMERICAL RESULTS AND DISCUSSION

4.1 Numerical validation

A bilinear viscous cohesive representation shown in Figure 1 is adopted to validate the calculations.

The matrix M coefficients were computed by a finite element model with six-node triangular elements using ANSYS[®]. The middle section was discretized into 100 equal divisions (i.e., N=100 in Figure 2).

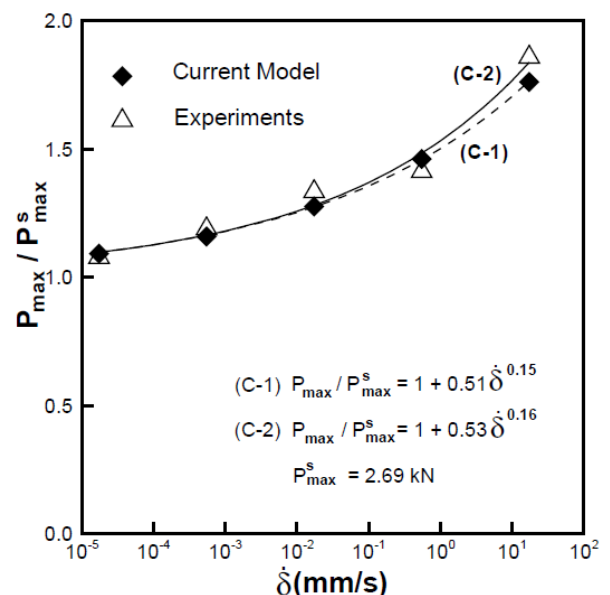
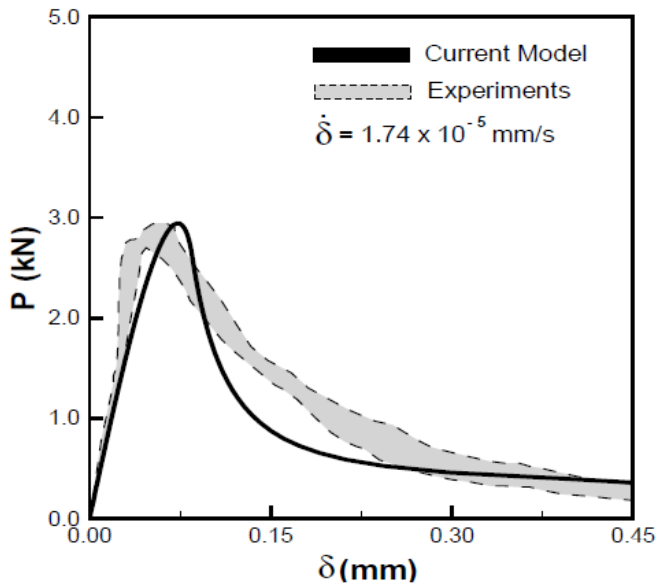
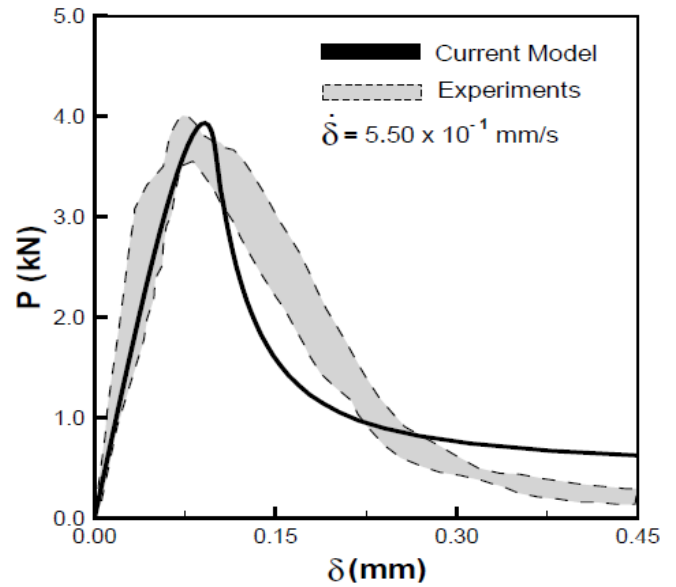


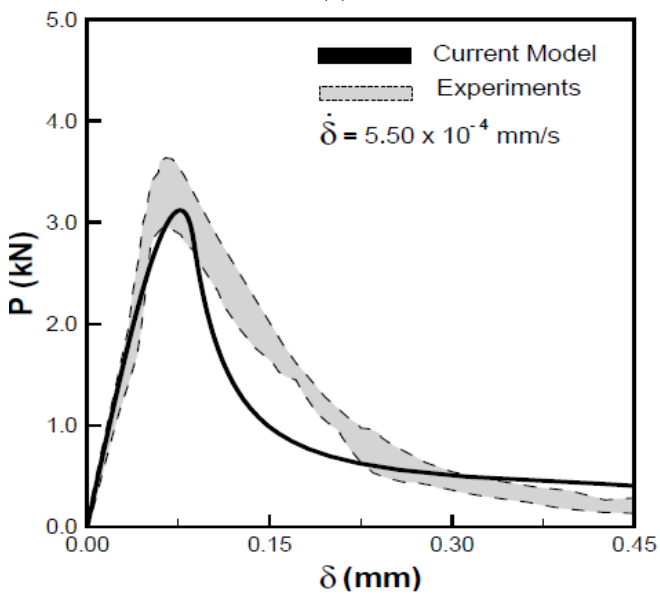
Figure 4. Curve adjust and comparison between predicted and experimental results at different load loading rates.



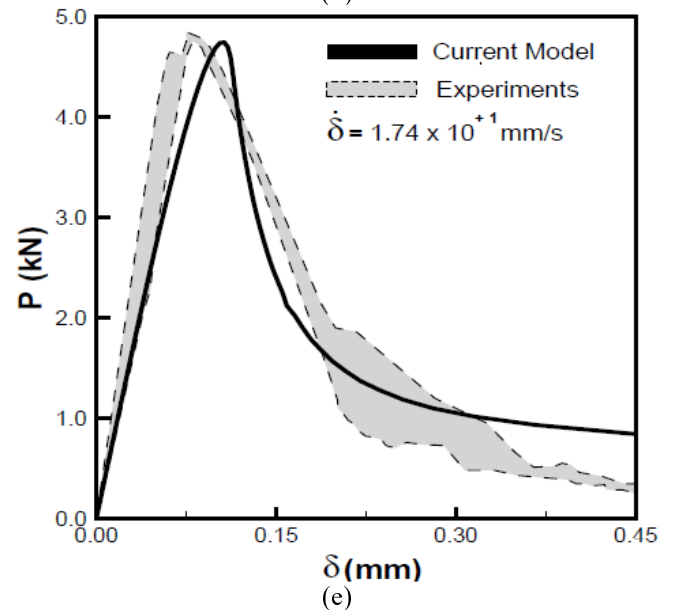
(a)



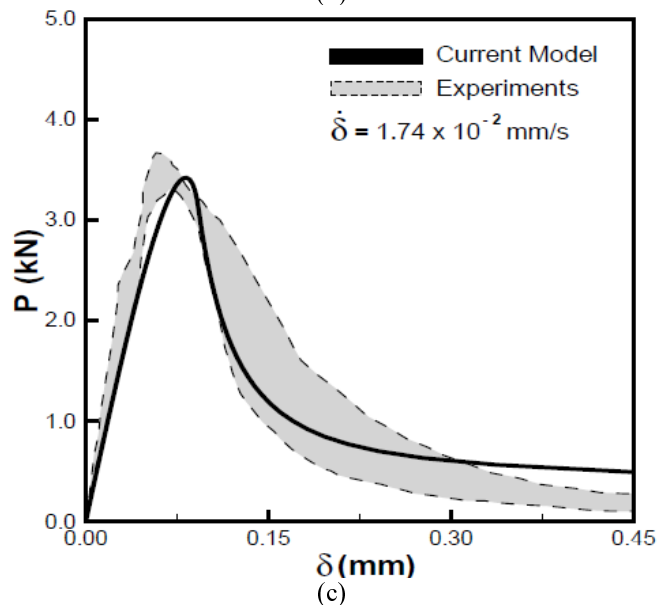
(d)



(b)



(e)



(c)

Figure 4. Load-displacement curves for the five loading rates applied in the tests.

The rate dependent index, $n = 0.16$, was obtained through curve fitting of the experimental non-dimensional peak load as a function of the loading applied rate. Subsequently the parameter $\dot{w}_0 = 9.65 \times 10^{-2} \text{ mm/s}$ was computed in an inverse manner by curve fitting with a predefined value of n .

The comparison between numerical and experimental values for peak load is shown in Figure 4. Almost perfect agreement is shown for peak loads.

The comparison between complete load-displacement curves is shown in Figure 5 for the five loading rates applied in the tests. We observe that the proposed numerical model faithfully reproduces the experimental results.

4.2 Parametric study

Figure 5 shows the nondimensional load ($2P/BDf_t^s$) vs. the nondimensional displacement (δ/w_{ch}) curves for a large range nondimensional loading rates ($\dot{\delta}/\dot{w}_o$) and $n = 0.15$. As expected, it is clear a registered increase on the peak load for nonzero loading rate cases when compared with the corresponding static values (dashed line in the figure). Comparing static and nonzero loading rate results, we can conclude that rate effect induces a slightly more brittle behavior, dictated by a slightly higher relative displacement at peak.

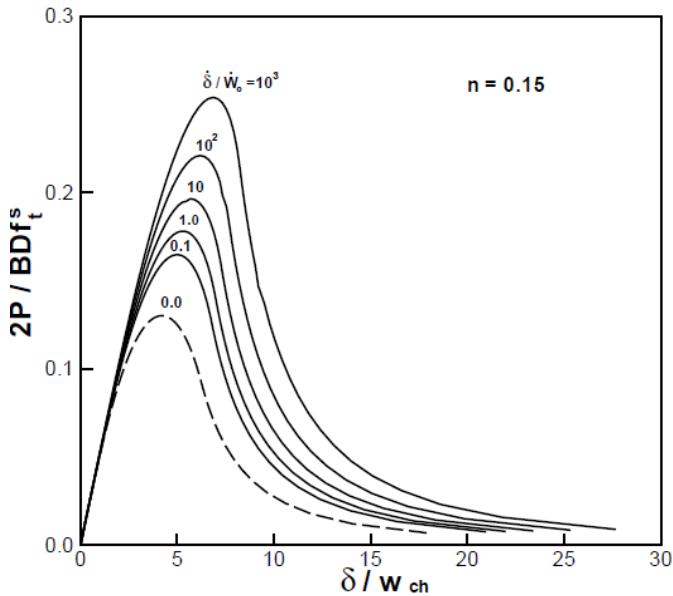


Figure 5. Nondimensional load vs. nondimensional displacement curves for $n = 0.15$.

Figures 6(a) and 6(b) point out the model trends on peak load and fracture energy, respectively, by different values of n and increasing loading rate. As seen in these figures, peak load and fracture energy increase monotonically with an increasing loading rate. It is noteworthy that for a higher value of the index n ($n = 0.60$ in our example) the peak load and the apparent fracture energy are almost constant in an extent range of loading rates. Since n is a non-dimensional parameter that describes the degree of viscosity of the bulk material, it is probably related with the presence of water activity in the material porous network and fracture energy can be considered as a rate independent parameter only for a certain range of applied loading rate and for a certain free water content in the material pores.

5 CONCLUSIONS

We have presented a rate dependent cohesive model in the framework of a finite element smeared-crack-tip method. The methodology is validated against high strength concrete (HSC) beams in a three-point bend (TPB) test configuration. A parametric study

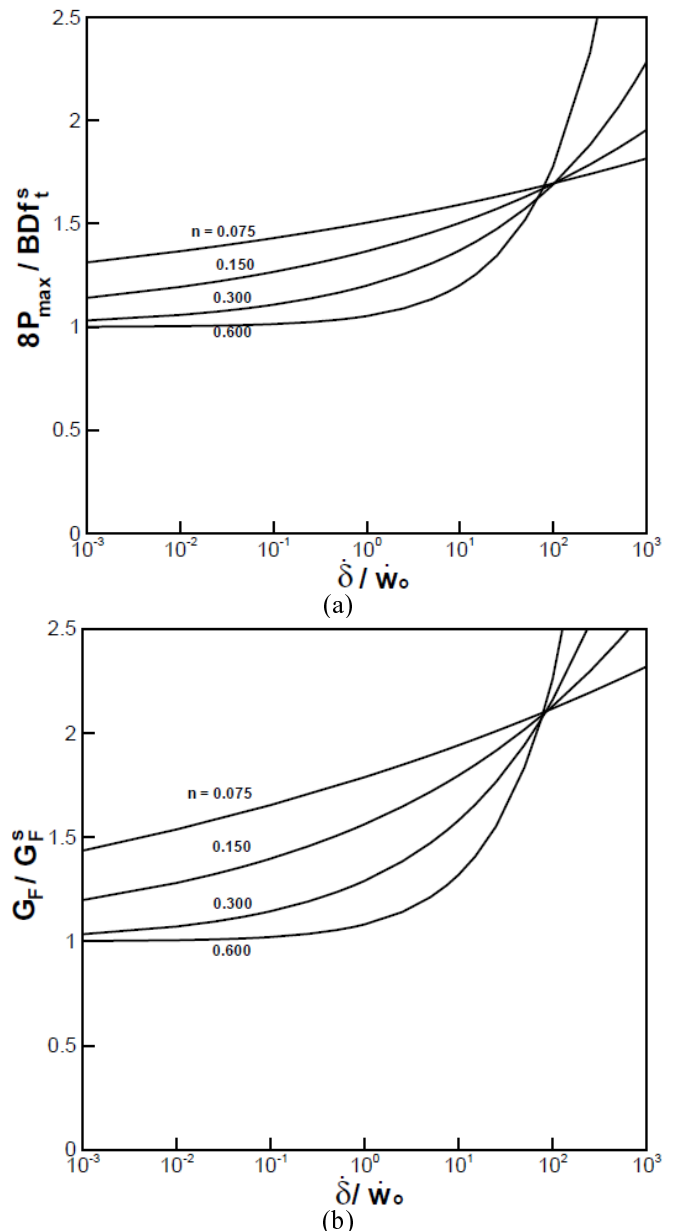


Figure 6. Nondimensional peak load and nondimensional work of fracture per unit area vs. the nondimensional loading rate for different values of n .

had also been realized to demonstrate how the parameters related with the time dependent model reflect the fracture response of the material.

Based on the findings of this research, the following conclusions can be drawn:

- The numerically obtained results match very well the experimental ones, particularly with respect to the maximum load, for the several loading rates used in the tests;
- The model can explicitly represent peak load and fracture energy dependence on the loading rate: both quantities increase as the loading rate increases;
- Numerical results obtained show that the model, despite its simplicity, provides a general approach that reflects the experimentally documented fact that the crack growth and fracture process depends on loading rate.
- As pointed out by numerical and experimen-

tal comparisons, the model seems promising and its further refinements can probably improve predictions on rate effect.

ACKNOWLEDGEMENTS

The authors gratefully acknowledge the financial support provided by the Brazilian institutions CAPES (grant CAPES/DGU 152-07, Process: BEX 1409/07-7) and FAPESP (grant 2006/01647-4), by the Spanish Ministry of Education through grant number MAT2006-09105 and by the UCLM Project (Ref.: 2008-BIN-2506).

REFERENCES

- Bažant, Z. P. 1990. Smeared-tip superposition method for nonlinear and time-dependent fracture. *Mechanics Research Communications*, 17(5), 343–351.
- Bažant, Z.P. & Gettu, R. 1992. Rate effects and load relaxation in static fracture of concrete. *ACI Materials Journal*, 89(5):456-468.
- Bažant, Z.P. & Jirásek, M. 1993. R-curve modeling of rate and size effects in quasibrittle fracture. *International Journal of Fracture*, 62(4):355-373.
- Bažant, Z. P. and Beissel, S. (1994). Smeared-tip superposition method for cohesive fracture with rate effect and creep. *International Journal of Fracture*, 65(33), 277–290.
- Bažant, Z.P. & Li, Y.N. 1997. Cohesive crack with rate-dependent opening and viscoelasticity I: mathematical model and scaling. *International Journal of Fracture*, 86(3):247-265.
- Bažant, Z.P., Caner, F.C., Adley, M.D & Akers, S.A. 2000. Fracturing rate effect and creep in microplane model for dynamics. *Journal of Engineering Mechanics*, 126(9):962-970.
- Bažant, Z.P. & Zi, G. 2003. Asymptotic stress intensity factor density profiles for smeared-tip method for cohesive fracture. *International Journal of Fracture*, 119(2):145-159.
- Brara, A. & Klepaczko, J.R. 2007. Fracture energy of concrete at high loading rates in tension. *International Journal of Impact Engineering*, 34(33):424-435.
- Guinea, G.V., Planas, J. & Elices, M. 1992. Measurement of the fracture energy using three-point bend tests: Part 1 - Influence of experimental procedures. *Materials and Structures*, 25(4):212-218.
- Elices, M., Guinea, G.V. & Planas, J. 1992. Measurement of the fracture energy using three-point bend tests: Part 3 - Influence of cutting the P- δ tail. *Materials and Structures*, 25(6):327-334.
- Elices, M., Guinea, G.V. & Planas, J. 1997. On the measurement of the fracture energy using three-point bend tests. *Materials and Structures*, 30(6):375-376.
- Gettu, R. & Bažant, Z.P. 1990. Fracture properties and brittleness of high-strength concrete. *ACI Materials Journal*, 87(6):608-618.
- Planas, J. 1986. Un nuevo método de análisis del comportamiento de una fisura cohesiva en Modo I. *Anales de Mecánica de la Fractura*, 3(1): 219-227.
- Planas, J. & Elices, M.A. 1991. Nonlinear fracture of cohesive materials. *International Journal of Fracture*, 51(2):139-147.
- Planas, J. & Elices, M. (1992). Asymptotic analysis of a cohesive crack: 1 - Theoretical background. *International Journal of Fracture* 55(2):153–177.
- Planas, J., Elices, M. & Guinea, G.V. 1992. Measurement of the fracture energy using three-point bend tests: Part 2 - Influence of bulk energy dissipation. *Materials and Structures*, 25(5):305-312.
- Planas, J. & Elices, M. (1993). Asymptotic analysis of a cohesive crack: 2. Influence of the softening curve. *International Journal of Fracture*, 64(3):221–237.
- Reinhardt, H.W. & Weerheijm, J. 1991. Tensile fracture of concrete at high loading rates taking into account of inertia and crack velocity effects. *International Journal of Fracture*, 51(1):31-42.
- RILEM 1985. Determination of the fracture energy of mortar and concrete by means of three-point bend tests. *Materials and Structures*, 18(4):285-290.
- Rossi, P., Van Mier, J.G.M., Boulay C. & Le Maou, F. 1992. The dynamic behavior of concrete: influence of free water. *Materials and Structures*, 25(153):509-514.
- Rossi, P., Van Mier, J.G.M., Toutlemonde, F. & Le Maou, F. 1994. Effect of loading rate on the strength of concrete subjected to uniaxial tension. *Materials and Structures*, 27(169):260-264.
- Ruiz, G. 2001. Propagation of a cohesive crack crossing a reinforcement layer. *International Journal of Fracture*, 111(3): 265-282.
- Ruiz, G., Zhang, X.X., Del Viso, J.R., Yu, R.C., & Carmona, J.R. 2008. Loading rate effect on the fracture behavior of high strength concrete. *Anales de Mecánica de la Fractura*, 25(2): 793-798.
- Zhang, X.X., Ruiz, G., Yu, R.C., & Tarifa, M. 2009. Fracture behavior of high-strength concrete at a wide range of loading rates. *International Journal of Impact Engineering*, 36(10): 1204-1209.